Progress In Electromagnetics Research, Vol. 178, 13–36, 2023

A Novel Noncontact Ku-Band Microwave Radiometer for Human Body Temperature Measurements

Hang Tian[1], Xiaodong ZhuGe[1], Anyong Hu[1], Qingli Dou[2, *], and Jungang Miao[1, *]

Abstract—In emergency departments and ICUs, a novel noncontact thermometer is urgently required to measure physical temperatures through common clothing to accomplish body temperature precise measurement for critical patients. Hence, a Ku band digital auto gain compensative microwave radiometer is proposed to get a higher theoretical temperature measurement sensitivity than a Dicke radiometer, benefit miniaturization design, and reduce attenuation caused by common clothing. Meanwhile, a novel compensation method for receiver calibration is proposed to improve temperature sensitivity under non-ideal conditions, and the revised systematic calibration method is elaborated. Furthermore, in order to invert body physical temperatures through clothing, a microwave thermal radiation transmission model of clothed human body is constructed, and the microwave radiation apparent temperature equation of clothed human body is derived. Importantly, three groups of experiments are set up to confirm the designed radiometer's performance, especially the biological tissue temperature measurement. Results show that: 1) the designed radiometer has high temperature sensitivity and accuracy for unsheltered targets; 2) amplitude attenuation caused by cotton cloth for Ku band microwave is much smaller than that for infrared thermal radiation; 3) the designed radiometer can track physical temperatures of targets (such as water and swine skin tissue) sheltered or covered by cotton cloth relatively accurately. In conclusion, our designed Ku band microwave radiometer is certificated to have outstanding performance in temperature measurement for biological tissue through common clothing, which can be developed into a promising product in medical monitoring.

1. INTRODUCTION

In emergency departments (EDs) and ICUs of hospitals, there exist a large number of critical patients. A lot of them suffer from emergent diseases encounter serious traffic accidents or accidents caused by other harsh environments, making these patients weak and seriously ill. Due to pathogenetic conditions, restraints, sedation, and other factors, most of them cannot cooperate with doctors to take vital signs independently, even they have no time to wait to measure body temperatures by undressing with assistance of medical staffs. Therefore, the contact temperature measurement by a mercurial thermometer is dangerous and inconvenient. For examples, when the oral temperature is measured by a mercurial thermometer, the mercurial thermometer is easy to be bite off; when the anal temperature is measured, the condition of the patient's fecal incontinence may exist, so that the mercurial thermometer may be polluted, and the measurement may be affected; when the axillary temperature is measured, there exists the condition that some critical patients cannot move and need assistance from medical staffs. Moreover, most environments where diseases occur are harsh, so deviations made by infrared thermometers for human forehead temperature measurements to indicate body temperatures become large. For example, when the outdoor environment temperature is below

Received 25 April 2023, Accepted 2 August 2023, Scheduled 14 August 2023
* Corresponding authors: Qingli Dou (douqingli@163.com), Jungang Miao (jmiaobremen@buaa.edu.cn).
[1] School of Electronics and Information Engineering, Beihang University, Beijing, China. [2] Emergency Department, People's Hospital of Shenzhen Baoan District, Shenzhen, China.

0°C, their forehead temperatures will be very low if people stay outside long time, so that their forehead temperatures cannot reflect changes of their body temperatures in a long period of time. Such data cannot be used as evidences for doctors to determine patients' conditions. For temperature measurement requirements of critical patients in ICUs and isolation wards, such as the diagnosis and treatment of infectious diseases, doctors also hope to use non-contact devices to measure and monitor vital signs of patients round the clock, to assist patients in treatment and reduce the chance of doctors being infected. Since many patients with infectious diseases cannot keep their heads still for a long time when they are in bed, there will be large deviations in measuring forehead temperatures using an infrared thermometer when being unattended. Thus, for these patients, doctors are trying to use other body parts as new temperature measuring points. It is noted that there exist abundant muscles, fat, and numerous organs in the torso, which can produce a lot of heat via metabolic pathways. And critical patients above often wear clothes or stay in bed for a long time in ICUs, so that the torso skin is close to clothes or bedding, forming a relatively closed environment, resulting in less heat dissipation of the patient 's torso. It is confirmed by experiments that there is no significant difference between the torso waist temperature and the axillary temperature under this condition. For such patients, doctors also want to use the torso covered with clothes or quilts as a new temperature test point. As mentioned, since mercurial thermometers and infrared thermometers cannot meet requirements in EDs and ICUs of hospitals, it is urgent to develop a novel thermometer as a complement, which can measure patients' forehead temperatures directly or patients' axilla or torso temperatures through clothes or quilts, and then calculate body temperatures by corresponding them to equivalent axillary temperatures of the human body with an algorithm.

Hence, in order to satisfy the needs above, a novel non-contact Ku band microwave radiometer is proposed for human body temperature measurement in this work. Importantly, the reason for choosing the Ku microwave band of our designed microwave radiometer is that, compared with the infrared band, multiple clothing materials have much smaller attenuation to microwave [1, 2], and also it has benefit for miniaturization.

Here, the design goal in this work is different from [3–8]. Reasons for choosing Ku band are explained below. According to the research of Gabriel et al. [11–13] on electromagnetic properties of human tissues in microwave band, when the frequency is higher than 9 GHz, penetration depths of both dry skin and wet skin are less than the maximum average skin thickness of 4.5 mm, as shown in Fig. 1. Although microwave radiometers with frequencies above 9 GHz have not been widely used in medical radiation measurements in recent years, many scholars have made active explorations since the 1970s. In [14], the theory of microwave radiometry of biological systems is outlined. An X–band microwave radiometer of the correlation radiometer has been built. Preliminary experiments were performed on different parts of a human subject, including head, hand, and back. In [15–17], a high sensitivity radiometer operating at 9 GHz was used for investigations on breast cancer patients and on patients with tumors of various localizations and histologic types. In [18], more than a hundred

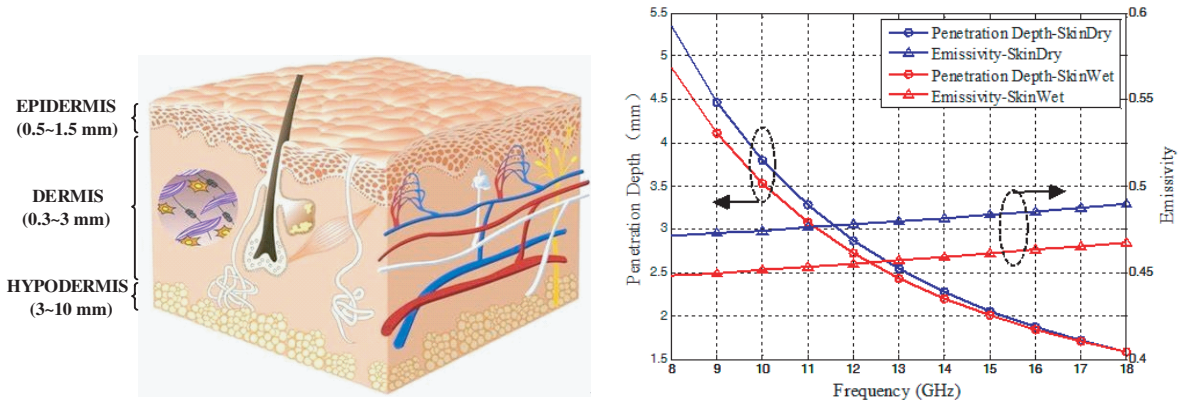

Figure 1. (a) Human skin model [2, 9, 10]; (b) Penetration depth and Emissivity of Human Skin.

cases of thyroidal, osteoarticular, facial, or intracranial pathologies have been explored with microwave thermography at 9, 30, and 68 GHz. Deep lesions such as those of femoral head or lumbar spine, or cerebral tumors were detected. In [19], a scanning microwave thermograph with the band 9–10 GHz has been built, which produced a video display of the variations in the emission temperature of the human body. Preliminary medical studies on a number of patients suffering from occlusive vascular disease of the lower limbs have been launched. In [20], a microwave thermometer RT-20 was used to carry out the study for making a microwave temperature chart of the whole cows' body surface. In [21], a Ka band contact radiometer was studied theoretically and experimentally for the accuracy of human-body temperature measurements. In [22], a 10 $\sim$ 12 GHz microwave radiometer was used for early breast cancer detection, and an analysis of physical principles of microwave thermography was made. In [23], a 12.5 GHz low-cost radiometric temperature sensor system was designed for biological tissue surface temperature measurements in the food industry, but its measurement sensitivity was not high. In [24], a microwave radiometer at 10.68 $\sim$ 10.70 GHz was designed for non-contact surface body temperature measurement with a horn antenna24. However, for the reason that its working bandwidth was only 20 MHz, its temperature sensitivity was not high. It is noteworthy that a horn antenna with high directivity was also adopted in our work the same as [24]. Referencing but better than these mentioned examples, considering the size of the horn antenna and waveguide, the working frequency band is selected in Ku band ultimately for miniaturization and integration of the designed microwave radiometer.

Next, the designed microwave radiometer is optimized into a digital auto gain compensative microwave radiometer, as shown in Fig. 2. Compared with the traditional Dicke radiometer, both of them use one internal reference source, while their operating principles and theoretical maximum sensitivities are quite different. The radiometer designed in this work has the same theoretical maximum temperature sensitivity as a total power radiometer, but the receiver structure is simpler than a Dicke radiometer so that the synchronous demodulator is not used. Until now, many research institutions in China have also used digital auto gain compensative technique to improve sensitivities of microwave radiometers, which is widely used in priority projects such as ground object detections and astronomical observations [25, 26].

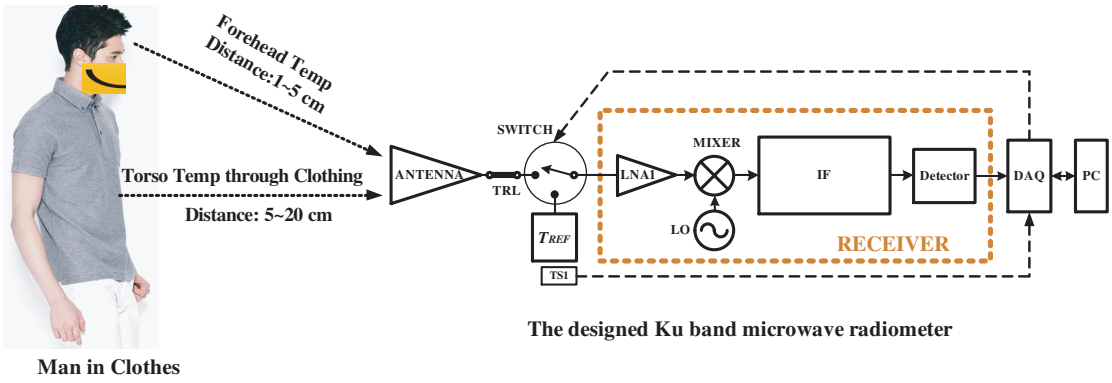

Figure 2. Block diagram of the designed digital auto gain compensative microwave radiometer.

2. MATERIALS AND METHODS

2.1. Working Principle of Digital Auto Gain Compensative Microwave Radiometer

The system structure and photograph of the digital auto gain compensative microwave radiometer designed in this work are shown in Fig. 2 and Fig. 5, respectively. The main body is a super-heterodyne receiver instead of a direct-conversion receiver. Owing to high costs of Ku band microwave elements, the noise power of the measured target is down-converted to intermediate frequency (IF) band through a superheterodyne receiver, so that related components are easy to obtain and have low cost. A reference noise source T_{REF} and microwave electronic switch **SWITCH** are added between the horn antenna and

the super-heterodyne receiver to smooth gain fluctuations of the radiometer. The data acquisition board **DAQ** is used to control data flows of the radiometer, collect and store output voltage data from the detector. **TRL** is a short coaxial transmission line used to test targets with different sizes. During the measurement process, the radiometer receiver is periodically switched between T_{REF} and the antenna by means of **SWITCH**.

As shown in Fig. 2, assuming that equivalent noise temperature of the super-heterodyne receiver is T_{REC} [27], T_{REC} can be determined by the following formula:

$$T_{REC} = T_{RF} + \frac{T_M}{G_{RF}} + \frac{T_{IF}}{G_{RF}G_M} + \dots \tag{1}$$

Here, G_{RF} is the power gain of Ku band low noise amplifier LNA1, T_{RF} the equivalent input noise temperature of LNA1, G_M the RF-to-IF power gain of MIXER, T_M the equivalent input noise temperature of MIXER, and T_{IF} the equivalent input noise temperature of IF band circuits.

When the electronic switch **SWITCH** is added, the equivalent noise temperature T'_{REC} of the receiver can be expressed as

$$T'_{REC} = (L_S - 1)T_{SWITCH} + L_S \bullet T_{REC} \tag{2}$$

Here, T_{SWITCH} is the physical temperature of **SWITCH**, and L_S is the loss factor of **SWITCH**.

Assume that antenna temperature T_A becomes T_{IN} after entering into **SWITCH** through **TRL**. Expressions of T_A and T_{IN} are given in Section 2.4. When the antenna is connected to the receiver by **SWITCH**, the output voltage (V_{OUTIN}) of the radiometer is

$$V_{OUTIN} = G_S(T_{IN} + T'_{REC}) \tag{3}$$

When the noise source T_{REF} is connected to the receiver by **SWITCH**, the output voltage (V_{OUTR}) of the microwave radiometer is

$$V_{OUTR} = G_S(T_{REF} + T'_{REC}) \tag{4}$$

Here, G_S (V/K) is the total system gain including the detector voltage sensitivity.

When the system gain G_S changes to G'_S with time, assuming that the time is so short that T_{REF}, T_{IN}, and T'_{REC} are not changed. At this time, when T_{REF} or the antenna is connected to the receiver, output voltages of the radiometer respectively are:

$$V'_{OUTR} = G'_S\left(T_{REF} + T'_{REC}\right) \tag{5}$$

$$V'_{OUTIN} = G'_S\left(T'_{IN} + T'_{REC}\right) \tag{6}$$

Here, to distinguish measured results, T_{IN} is written as T'_{IN}.

Then the output voltage corresponding to T'_{IN} is compensated when the system gain changes. The compensation formula is:

$$V''_{OUTIN} = \frac{V_{OUTR}}{V'_{OUTR}}V'_{OUTIN} = G_S\left(T'_{IN} + T'_{REC}\right) \tag{7}$$

Finally, T'_{IN} is determined by

$$T'_{IN} = \frac{V''_{OUTIN} - V_{OUTR}}{G_S} + T_{REF} \tag{8}$$

Here, G_S is solved according to Equation (22).

2.2. Design of Microwave Radiometer

2.2.1. Antenna of Microwave Radiometer

In noncontact human body temperature measurements, a horn antenna with high directionality is selected [24] to reduce environment noise contributions to the radiometer, which is a standard gain horn with 15 dBi gain. It should be noted that the horn antenna used in this design is not the final horn antenna style, and its physical size can be reduced by a variety of methods by referencing [28–36]. However, the requirement to reduce its physical size or not is determined by specific clinical applications.

The reason that a standard gain horn with 15 dBi gain is selected in this work is that its radiation pattern and other indicators are standard, and its performance is appropriate for clinical applications discussed in this paper. Its performance can be queried in many websites and companies [37, 38]. In processes of the performance verification and temperature inversions for the designed microwave radiometer, the error caused by the antenna performance uncertainty can be reduced, and the temperature measurement accuracy can be improved. The basic parameters and photograph of the antenna are shown in Fig. 3 and Table 1.

Table 1. Devices' basic parameters of the designed microwave radiometer.

Symbol	Basic Parameters
Antenna	RF Frequency: Ku band; Radiation Efficiency η_l: 94.5% at 14 GHz Size: 50 mm (L) × 40 mm (W) × 85 mm (H)
TRL (Transmission Line)	RF Frequency: DC ∼ 18 GHz; VSWR: ≤ 1.1; Insertion loss: 0.3 ∼ 0.4 dB
SWITCH	RF Frequency: 10 ∼ 20 GHz; Insertion Loss: 1.8 dB

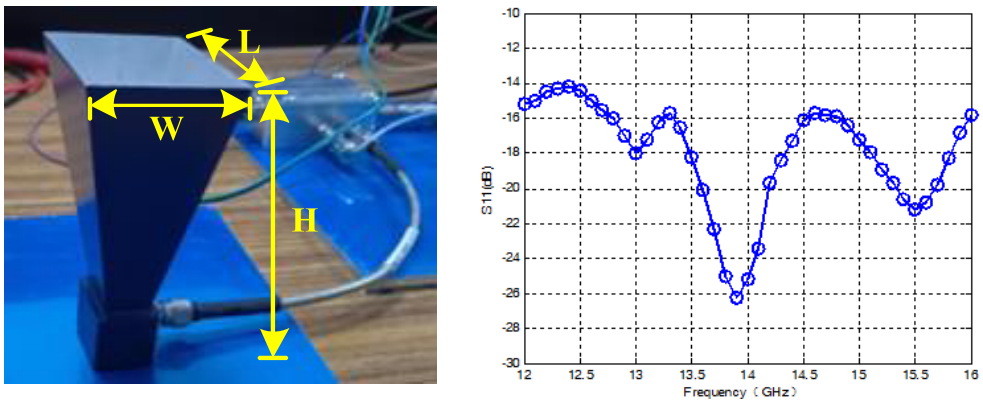

(a) (b)

Figure 3. Antenna parameters. (a) Antenna in the design; (b) S_{11} (dB) measured.

2.2.2. Switching Time of Microwave Switch

Although calibration devices of the designed radiometer are similar to the Dicke radiometer, their calibration principles are quite different. For the Dicke radiometer, the Dicke switch needs to be switched twice over the entire integration time τ due to the synchronous demodulator, so that the switching time t_s of the Dicke switch is $t_s = \tau/2$ [27].

For the designed radiometer in this work, the microwave switch needs to be switched only once over τ. After the output voltage signals have been integrated over τ, the analog to digital (AD) converter on the **DAQ** board samples them. After sampling is completed, the switch is switched to other ports. The switch completes the above repeated action under the control of the **DAQ** board. Therefore, the switching time t_{SWITCH} of **SWITCH** is:

$$t_{SWITCH} = \tau + n \bullet \tau_{AD}, \quad n = 1, 2, 3, \ldots \tag{9}$$

where τ_{AD} is the sampling time of the AD converter, and n is a positive integer. $n \bullet \tau_{AD}$ means that the AD converter samples the output voltage signals for n times after the output voltage signals have been integrated over time τ.

2.2.3. Microwave Internal Reference Noise Source

The microwave reference noise source T_{REF} is a specially designed and manufactured matched load, whose equivalent noise temperature T_{REF} is given by [39]

$$T_{REF} = \left(1 - |\Gamma_{REF}|^2\right) T_r \tag{10}$$

Here, T_r and Γ_{REF} are the physical temperature and terminal reflection coefficient of the microwave internal reference noise source, respectively. T_r is measured by a RTD PT100, so as to avoid using temperature-controlled equipment with huge volume. Fig. 4(a) shows the terminal reflection coefficient Γ_{REF} of the microwave reference noise source.

2.2.4. Receiver Predetection Total Gain

The receiver predetection total gain G_{HF} plays a critical role in obtaining excellent system performance. In order to guarantee that the radiometer works well, two important criteria must be met for G_{HF}: First, it must be large enough to ensure the noise figure required by the receiver; second, the power detector must operate in the square law region.

To satisfy the first key criterion, G_{HF} must meet the following equation:

$$G_{HF} \geq A\frac{\Delta T_{V\min}}{\Delta T_{\min}} \tag{11}$$

Here, A is a constant determined by the specific receiver and generally 10; $\Delta T_{\min}$ is the temperature measurement sensitivity of the radiometer; $\Delta T_{V\min}$ is the minimum detectable temperature for the square law detector and terminal amplifier, which is expressed as:

$$\Delta T_{V\min} = \frac{2}{C_d \bullet \sqrt{k}} \bullet \sqrt{T_0 R_V F_V} \bullet \frac{\sqrt{B_{LF}}}{B} \tag{12}$$

where C_d is the sensitivity of the square law detector (V/W); R_V is the low frequency resistance of the detector (Ω); F_V is the noise figure of the terminal amplifier (DC voltage amplifier); B_{LF} is the bandwidth (Hz) of the terminal amplifier; B is the noise bandwidth (Hz) of the receiver; k is the Boltzmann constant; $T_0 = 290\,\mathrm{K}$.

In order to satisfy the second key criterion, the operating point should be selected appropriately according to the characteristic curve of the detector, so that the maximum output power of IF band circuits can be in the square law region of the detector. After the maximum allowed input power P_{IF} of the detector is determined, G_{HF} is determined as

$$G_{HF} \leq \frac{P_{IF}}{2kT_{sys}B} \tag{13}$$

where T_{sys} is the equivalent noise temperature of the radiometer.

In this work, a square law detector is used for the radiometer whose working band is $0.6 \sim 4\,\mathrm{GHz}$. The input power point $1.1\,\mathrm{mW} \sim 1.4\,\mathrm{mW}$ ($0.41 \sim 1.46\,\mathrm{dBm}$) is selected which is enough by referencing Table 2. A practical measurement and linear fitting were carried out, as shown in Fig. 4(b). The linearity of the detector is better than 0.9995 at 2.7 GHz.

Table 2. Values of equivalent noise temperatures.

Symbol	Basic Parameters
T'_{REC}	$692.6481\,\mathrm{K}$
T_{IN}	$289.7775 \sim 294.727\,\mathrm{K}$
$T_{sys} = T'_{REC} + T_{IN}$	$982.4256 \sim 987.3751\,\mathrm{K}$
$P_{SYSIN} = k \bullet (T'_{REC} + T_{IN}) \bullet B$	$-73.2375 \sim -73.2157\,\mathrm{dBm}$

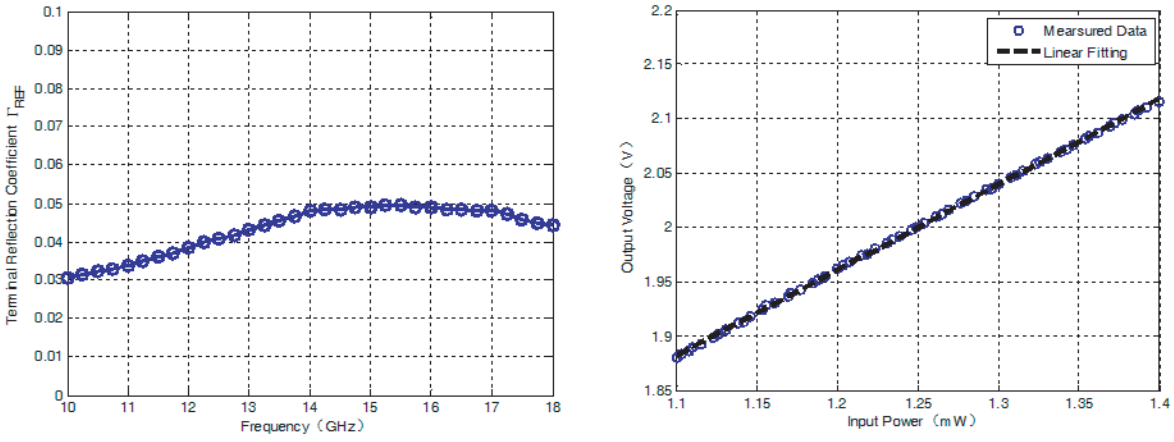

(a) (b)

Figure 4. (a) The terminal reflection coefficient Γ_{REF} of the microwave internal reference noise source. (b) Output Voltage VS Input Power at 2.7 GHz for the detector.

By substituting the selected power point and the parameters of the device in this work into Equation (11) $\sim$ (13), 51.2 dB $\leq G_{HF} \leq$ 68.7 dB is obtained. In addition, the IF band circuits should provide an extra gain of about 10 dB to compensate the loss.

2.2.5. Basic Performance of Designed Microwave Radiometer Receiver

The development of hardware circuits went through two stages for the designed Ku band microwave radiometer. In the first stage, discrete circuit modules were assembled to verify feasibility and performance of the designed radiometer, as shown in Fig. 5(a). In the second stage, miniaturization design was made, as shown in Fig. 5(b). The measured gain and noise figure of the radiometer are shown in Figs. 5(c) and (d). Values of equivalent noise temperatures are listed in Table 2. B is about 3.5 GHz. Here, the emissivity of the skin is regarded as 0.48 [11–13], and temperature range for calculation is 30 $\sim$ 42°C.

2.3. Temperature Measurement Sensitivity Analysis and Revised Calibration Method under Non-Ideal Conditions

In this section, in the first place, the maximum temperature sensitivity of the designed radiometer under ideal conditions is given and compared with classical types of microwave radiometers. Then, the temperature sensitivity of the designed radiometer under non-ideal conditions is analyzed. Since the physical temperature of the internal reference noise source T_{REF} is measured in real time rather than at a fixed temperature point, the temperature sensitivity of the designed radiometer would get worse by only applying the ideal calibration method proposed by Equations (3)–(8). In order to improve the temperature sensitivity of the designed radiometer, a novel compensation method related to the physical temperature of T_{REF} is proposed for receiver calibration, and the systematic calibration method for the designed radiometer is given in detail.

2.3.1. Temperature Sensitivity of Designed Radiometer under Ideal Conditions

The radiation measurement sensitivity of a microwave radiometer is affected by both noise uncertainty ΔT_N and gain uncertainty ΔT_G. The radiation measurement sensitivity of a microwave radiometer can be expressed as [27]:

$$\Delta T = \sqrt{(\Delta T_N)^2 + (\Delta T_G)^2} = \left[T_{sys}^2 \bullet \frac{a}{B\tau} + T_{NE}^2 \bullet \left(\frac{\Delta G}{G} \right)^2 \right]^{1/2} \tag{14}$$

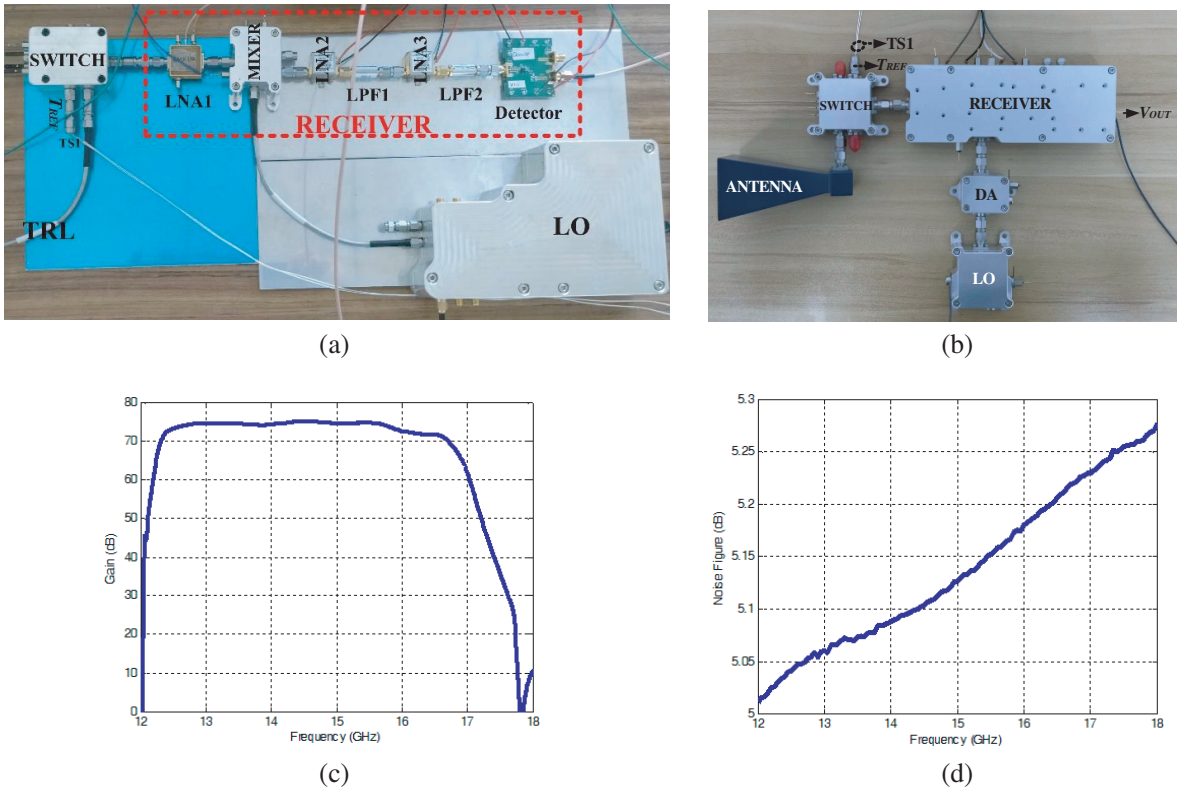

Figure 5. Designed Ku band microwave radiometer. (a) Photograph of the designed radiometer assembled with discrete modules; (b) Photograph of the designed radiometer after miniaturization; (c) Receiver predetection total gain measured; (d) Noise figure measured.

Here, τ is the integration time, a a constant related to the receiver, ΔG the system gain fluctuation, and T_{NE} the weight coefficient related to system noise temperature for ΔG.

Since t_{SWITCH} is longer than τ for the designed radiometer, the uncertainty caused by ΔT_N is the same as that in a total power microwave radiometer (that is, $a \approx 1$), and ΔT_G can be reduced to zero theoretically after compensation, so that the designed radiometer has a high temperature measurement sensitivity. Table 3 shows the temperature sensitivity expressions of several typical microwave radiometers.

Table 3. Temperature sensitivities of typical microwave radiometers.

Type of radiometer	$\Delta T_N = \frac{aT_{sys}}{\sqrt{B\tau}}$	$\Delta T_G = T_{NE} \bullet \frac{\Delta G}{G}$
Total power microwave radiometer	$a = 1$	$T_{sys} \bullet \frac{\Delta G}{G}$
Dicke microwave radiometer	$a = 2$	$(T_A - T_R)\frac{\Delta G}{G}$ [17]
Digital auto gain compensative radiometer	$a \approx 1$	$T_{sys} \bullet \frac{\Delta G}{G} \to 0$

2.3.2. Analysis of Temperature Sensitivity and a Novel Compensation Method under Non-Ideal Conditions for Designed Radiometer

As mentioned above, the ideal temperature sensitivity of the designed radiometer is the same as that of a total power radiometer under ideal conditions τ. But under non-ideal conditions, the physical temperature of the internal reference noise source may change from T_{REF} to $T_{REF} + \Delta T_{REF}$; the system

equivalent noise temperature may change from T'_{REC} to $T'_{REC} + \Delta T_{REC}$; and the system gain changes from G_S to $G'_S = G_S + \Delta G_S$ between two adjacent radiometer calibration cycles. Then Equations (5) and (6) can be rewritten as:

$$V'_{OUTR} = G'_S \left(T_{REF} + \Delta T_{REF} + T'_{REC} + \Delta T_{REC}\right) = G'_S \left(1 + \frac{\Delta T_{REF} + \Delta T_{REC}}{T_{REF} + T'_{REC}}\right)\left(T_{REF} + T'_{REC}\right) \quad (15)$$

$$V'_{OUTIN} = G'_S \left(T'_{IN} + T'_{REC} + \Delta T_{REC}\right) = G'_S \left(1 + \frac{\Delta T_{REC}}{T'_{IN} + T'_{REC}}\right)\left(T'_{IN} + T'_{REC}\right) \quad (16)$$

Here, $(\Delta T_{REF} + \Delta T_{REC})/(T_{REF} + T'_{REC})$ and $\Delta T_{REC}/(T'_{IN} + T'_{REC})$ can be regarded as gain fluctuations caused by equivalent noise temperature changes. Then Equation (7) becomes:

$$V''_{OUTIN} = G_S \left(1 - \frac{\Delta T_{REC} \bullet (T'_{IN} - T_{REF}) + \Delta T_{REF} \bullet (T'_{IN} + T'_{REC})}{\left(T'_{IN} + T'_{REC}\right)\left(T_{REF} + T'_{REC} + \Delta T_{REF} + \Delta T_{REC}\right)}\right)\left(T'_{IN} + T'_{REC}\right) \quad (17)$$

Equation (17) is the result of the real situation after the correction process on the basis of Equations (3) and (4) and Equations (5) and (6). In Equation (17), let

$$\frac{\Delta G_{S1}}{G_S} = \frac{\Delta T_{REC} \bullet (T'_{IN} - T_{REF}) + \Delta T_{REF} \bullet (T'_{IN} + T'_{REC})}{\left(T'_{IN} + T'_{REC}\right)\left(T_{REF} + T'_{REC} + \Delta T_{REF} + \Delta T_{REC}\right)} \quad (18)$$

Here, Equation (18) can be regarded as gain fluctuations caused by equivalent noise temperature changes after correction. Thus, by only applying the ideal calibration method by Equations (3)–(8), the temperature sensitivity of the designed radiometer is:

$$\begin{aligned} \Delta T_1 &= T_{SYS} \left[\frac{1}{B\tau} + \left(\frac{\Delta G_{S1}}{G_S}\right)^2\right]^{1/2} \\ &= T_{SYS} \left[\frac{1}{B\tau} + \left(\frac{\Delta T_{REC} \bullet (T'_{IN} - T_{REF}) + \Delta T_{REF} \bullet (T'_{IN} + T'_{REC})}{\left(T'_{IN} + T'_{REC}\right)\left(T_{REF} + T'_{REC} + \Delta T_{REF} + \Delta T_{REC}\right)}\right)^2\right]^{1/2} \end{aligned} \quad (19)$$

According to Equation (19), the temperature sensitivity of the designed radiometer is shown in Fig. 6(a). Here, parameters used in Equations (18) and (19) come from Table 2. As shown in Fig. 6(a), when $\Delta T_{REF} = 0\,\mathrm{K}$ and ΔT_{REC} varies between 0 and 30 K, the temperature sensitivity of the designed radiometer varies between 0.0155 K and 0.2 K only. It means that when ΔT_{REF} is maintained at a fixed temperature point, the ideal calibration method is effective to reduce fluctuations caused by ΔG_S and ΔT_{REC}, and keeps the digital auto gain compensative microwave radiometer working with a high temperature sensitivity. When $\Delta T_{REF} \neq 0\,\mathrm{K}$ and varies from 0.1 K to 1 K, with ΔT_{REC} varying from 0 to 30 K, the temperature sensitivity of the designed radiometer varies from 0.1 K to 1.2 K. It can be seen that the temperature sensitivity of the designed radiometer is quite sensitive to ΔT_{REF} and gets worse with the existence of ΔT_{REF} by only applying the ideal calibration method, so that an external calibration source must be applied to reduce ΔG_{S1} repeatedly according to Equation (22) to maintain a high sensitivity of the designed radiometer.

In order to reduce the influence of $\Delta G_{S1}/G_S$ on the temperature sensitivity ΔT_1, a novel compensation method is proposed here. Because ΔT_1 is sensitive to ΔT_{REF}, the influence of ΔT_{REF} on the temperature measurement sensitivity must be reduced. It is well known that ΔT_{REC} is difficult to measure accurately, whereas Δ_{REF} and $T_{REF} + \Delta T_{REF}$ can be measured by RTD PT100 easily, so that Equation (17) can be revised as

$$V''_{OUTIN} + G_S \bullet \Delta T_{REF} = G_S \left(1 - \frac{(\Delta T_{REF} + \Delta T_{REC}) \bullet (T'_{IN} - T_{REF} - \Delta T_{REF})}{\left(T'_{IN} + T'_{REC}\right)\left(T_{REF} + T'_{REC} + \Delta T_{REF} + \Delta T_{REC}\right)}\right)\left(T'_{IN} + T'_{REC}\right) \quad (20)$$

Then, the temperature sensitivity of the designed radiometer becomes:

$$\Delta T_2 = T_{SYS} \left[\frac{1}{B\tau} + \left(\frac{(\Delta T_{REF} + \Delta T_{REC}) \bullet (T'_{IN} - T_{REF} - \Delta T_{REF})}{\left(T'_{IN} + T'_{REC}\right)\left(T_{REF} + T'_{REC} + \Delta T_{REF} + \Delta T_{REC}\right)}\right)^2\right]^{1/2} \quad (21)$$

According to Equation (21), the temperature sensitivity ΔT_2 is shown in Fig. 6(b). As can be seen from Fig. 6(b), ΔT_2 becomes less sensitive to ΔT_{REF} and is greatly decreased when ΔT_{REF} exists, so that the designed radiometer can work at a high temperature sensitivity 0.1 K with conditions $\Delta T_{REF} \leq 10.0\,\mathrm{K}$ and $\Delta T_{REC} \leq 15.0\,\mathrm{K}$ met after Equation (21) being applied compared with Equation (19). After Equation (17) is revised to Equation (20), the designed radiometer no longer has to be calibrated repeatedly by an external calibration source.

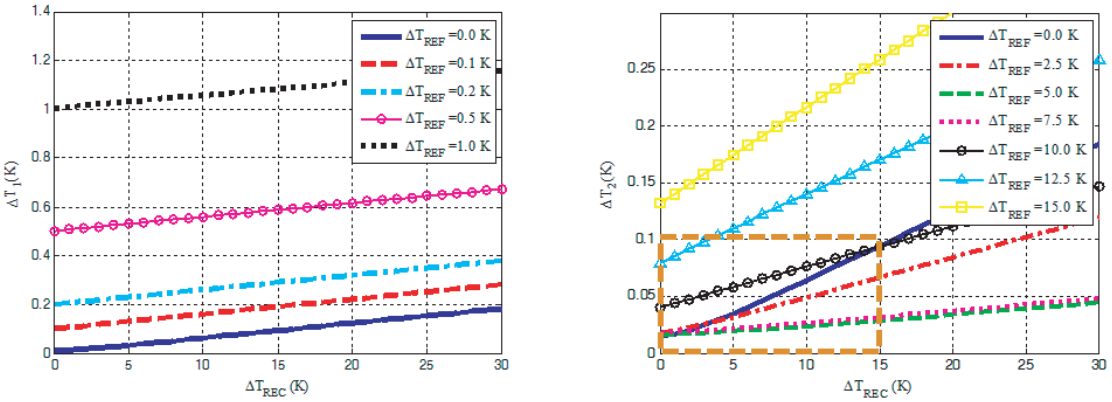

Figure 6. (a) The temperature sensitivity according to Equation (19); (b) The temperature sensitivity according to Equation (21).

2.3.3. Revised Calibration Method for the Designed Radiometer

In order to calculate T'_{IN}, G_S must be calculated with the help of an external calibration source whose equivalent noise temperature is T_{EREF} after the radiometer works stably, as shown in Fig. 7. Considering existences of ΔT_{REF} and ΔT_{REC}, the revised calibration method proposed is as follows:

Step (1) Control **SWITCH** to point to the antenna. The aperture of the antenna is focused on an external calibration source (T_{EREF} is fixed and should be different from T_{REF}), as shown in Fig. 7(a). T_{EREF} becomes T_{ERIN} after entering into **SWITCH** through **TRL**. T_{ERIN} can be calculated since parameters of **ANTENNA** and **TRL** are measured and definite, and the voltage $V_{OUTER} = G_S\,(T_{ERIN} + T'_{REC})$ output by the radiometer is recorded at the same time.

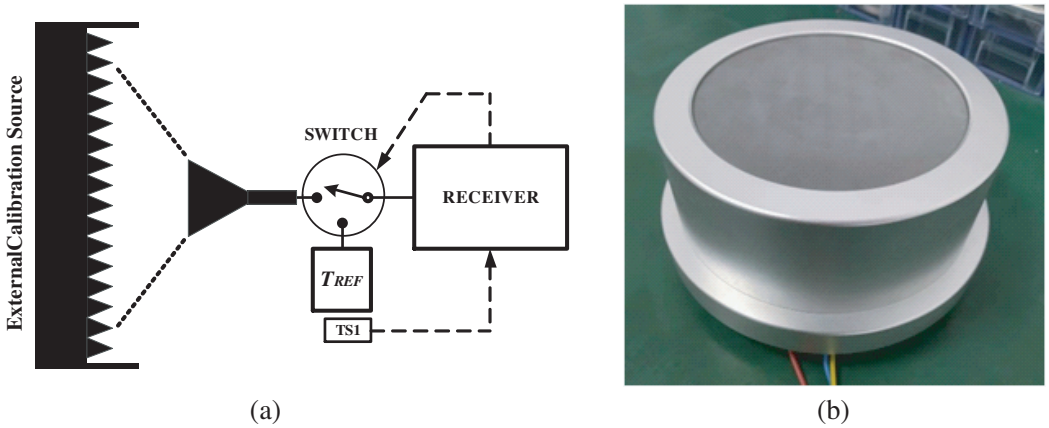

Figure 7. (a) Diagram of external calibration; (b) The external calibration source.

Step (2) Record T_{REF} and $V_{OUTR} = G_S\,(T_{REF} + T'_{REC})$ output by the radiometer when **SWITCH** points to the internal reference source T_{REF}.

Step (3) Calculate the initial gain G_S of the designed radiometer from records as

$$G_S = \frac{V_{OUTR} - V_{OUTER}}{T_{REF} - T_{ERIN}} \tag{22}$$

Step (4) After that, the antenna is aimed at the measured target for temperature measurements. Control **SWITCH** to switch between **ANTENNA** and T_{REF} periodically, and record T_{REF} and voltages output by the radiometer. Calculate V''_{OUTIN} according to Equations (5)–(7), and revise it according to Equations (20). Then calculate T'_{IN} according to Equation (8).

Step (5) When the conditions $\Delta T_{REF} \leq 10.0\,\mathrm{K}$ and $\Delta T_{REC} \leq 15.0\,\mathrm{K}$ are not met, repeat steps (1) $\sim$ (4) in sequence. Otherwise, only step (4) is needed to calculate T'_{IN}.

2.4. Temperature Inversion of Targets in Near Field

When a target is measured, the antenna temperature T_A can be solved from voltages output by the radiometer. The process of solving the apparent temperature from the antenna temperature T_A is called inversion of apparent temperature [40, 41]. The brightness temperature T_B of the target can be solved by subtracting the ambient scattered radiation temperature from the apparent temperature [42, 43]. And the target's physical temperature T_h can be solved from the target's brightness temperature T_B.

In this section, the method of temperature inversion for uncovered skin in near field is firstly presented, and then the microwave thermal radiation transmission model of clothed human skin is proposed and applied to the temperature inversion for clothed human skin.

2.4.1. Physical Temperature Inversion for the Uncovered Human Skin in Near Field

Assuming that the physical temperature of the measured target is T_h; the emissivity is ε_h; and the brightness temperature of the measured target is T_B, then the following relationship exists:

$$T_B = \varepsilon_h T_h \tag{23}$$

In the indoor environment, the apparent temperature of the human body T_{APH} is:

$$T_{APH} = \varepsilon_h T_h + (1 - \varepsilon_h)\, T_s = T_B + (1 - \varepsilon_h)\, T_s \tag{24}$$

In this work, a horn antenna with high directivity is selected, and the non-contact measurement distance is relatively close. Thus, when the antenna aperture is oriented in the direction of a specific part of a human body, T_{APH} can be considered as one constant within the detection range of the antenna. Ideally, the room ambient brightness temperature is consistent in all directions and is equal to T_s. Considering that an actual antenna is not ideal, T_A can be written as:

$$T_A = \left[\left(\eta_M T_{APH} + (1 - \eta_M)\, T_s\right)\eta_l + T_{pa}\,(1 - \eta_l)\right] \bullet \left(1 - |\Gamma|^2\right) \tag{25}$$

When T_A enters **SWITCH** through **TRL**, T_{IN} can be expressed as [18]:

$$T_{IN} = \left[\left(\eta_M T_{APH} + (1 - \eta_M)\, T_s\right)\eta_l + T_{pa}\,(1 - \eta_l)\right] \bullet \left(1 - |\Gamma|^2\right) \bullet \frac{1}{L} + \left(1 + \frac{|\Gamma|^2}{L}\right)\left(1 - \frac{1}{L}\right) T_{pl} \tag{26}$$

Here, for an antenna, η_l is its radiation efficiency; T_{pa} is its physical temperature; and Γ is its reflectivity coefficient. η_M is the weighting coefficient of the antenna for the measured target. For **TRL**, T_{pl} is its physical temperature, and L is its loss factor.

Thereby, for the inversion of physical temperature T_h of uncovered human skin or objects without shelter in near field, Equations (23)–(26) are adopted.

In the near field of the antenna, the weighting coefficient η_M is defined:

$$\eta_M = \frac{\iint\limits_{\Omega_T} F_n\,(\theta, \varphi)\, d\,\Omega}{\iint\limits_{4\pi} F_n\,(\theta, \varphi)\, d\,\Omega} \tag{27}$$

where $F_n(\theta, \phi)$ is the antenna weighting function, Ω the solid angle, and Ω_T the solid angle subtended by the measured target.

As the antenna almost works in near field, η_M is a function of the distance between the target and the antenna aperture, and it is related to the size and work frequency band of the antenna as well as the size of the target, but not invariable. The actual measurement for η_M is very tedious and cannot include all instances. Based on the above facts, the simulation method is adopted in this work to obtain η_M.

2.4.2. Physical Temperature Inversion for Clothed Human Skin in Near Field

When the human body is in common clothes or quilts, the apparent temperature distributions of the human body finally received by the radiometer are comprehensive. They can be described as radiation components, including radiation temperatures of clothing/quilt, human body, and surroundings which are finally incident upon the antenna aperture after repeated reflection and transmission at every interface.

In order to invert the physical temperature of human skin through clothing or quilts, a microwave thermal radiation transmission model of clothed human body is proposed based on the knowledge of microwave security [44]. According to the transmission model, the microwave radiation apparent temperature equation of clothed human body is derived, so that the physical temperature of human skin in clothes can be solved.

2.4.2.1. Microwave Thermal Radiation Transmission Model of Clothed Human Body

The microwave thermal radiation transmission model of clothed human body proposed in this work is shown in Fig. 8. The transmission model can be evolved into a 4-layer hierarchical structure, that is, air-clothing-air-human body. Fig. 8 shows the contribution of ambient radiation temperature, clothing radiation temperature, and human body radiation temperature to human body apparent temperature. The radiation transmission model will be analyzed in detail below.

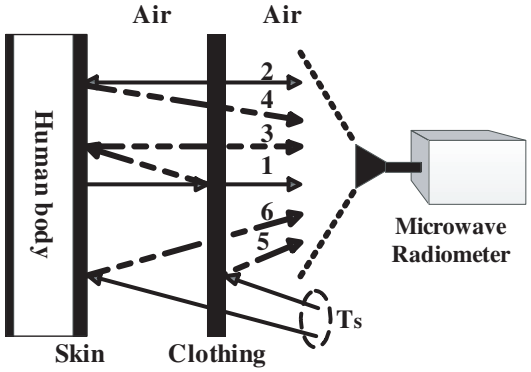

Figure 8. Microwave thermal radiation transmission model of clothed human body.

As shown in Fig. 8, the apparent brightness temperature of human body mainly includes three parts: first, the radiation temperature of clothing itself (2 in Fig. 8); second, the radiation temperature reflected by clothing coming from environment (5 in Fig. 8); third, radiation temperatures penetrating through clothing (1, 3, 4, 6 in Fig. 8). Among them, the third part is complicated, which includes the radiation temperature of human body itself (1 in Fig. 8) and the radiation reflected by human body coming from the equivalent environment temperature. The equivalent environment temperature includes the environment temperature penetrating through clothing and reflected by human body (6 in Fig. 8), the radiation temperature reflected by human body coming from clothing itself (4 in Fig. 8), and the radiation temperature reflected by clothing coming from human body (3 in Fig. 8). Therefore, the apparent brightness temperature of human body can be expressed by the following formula (the

human body transmittance is regarded as 0):

$$T_{APHS} = [\varepsilon_h T_h + T'_s \rho_h] t_c + \varepsilon_c T_c + \rho_c T_s = [\varepsilon_h T_h + (T_s t_c + \varepsilon_c T_c + \rho_c T_h)\rho_h] t_c + \varepsilon_c T_c + \rho_c T_s \quad (28)$$

Here, T_{APHS} is the apparent brightness temperature of human body, K; ε_h is the emissivity of the human body; t_c is the transmissivity of clothing; ρ_c is the reflectivity of clothing; T_h is the physical temperature of the human body, K; T_c is the physical temperature of clothing, K; T_s is the ambient temperature, K; T'_s is the equivalent ambient temperature, K.

2.4.2.2. Physical Temperature Inversion Equation for Clothed Human Skin

Considering that the actual antenna is not ideal, substitute Equation (28) into Equation (26), so that the antenna temperature T_{AHS} for human skin with shelter can be expressed as:

$$T_{AHS} = \left[\left(\eta_M T_{APHS} + (1 - \eta_M) T_s\right) \eta_l + T_{pa} (1 - \eta_l)\right] \bullet \left(1 - |\Gamma|^2\right) \quad (29)$$

When T_{AHS} enters **SWITCH** through **TRL**, it becomes T_{INHS}:

$$T_{INHS} = \left[\left(\eta_M T_{APHS} + (1 - \eta_M) T_s\right) \eta_l + T_{pa} (1 - \eta_l)\right] \bullet \left(1 - |\Gamma|^2\right) \bullet \frac{1}{L} + \left(1 + \frac{|\Gamma|^2}{L}\right) \left(1 - \frac{1}{L}\right) T_{pl} \quad (30)$$

Therefore, for the inversion of physical temperature T_h of human skin with shelter in near field, Equations (28)–(30) are adopted.

3. RESULTS

To verify the performance of the designed microwave radiometer, several measurement setups are introduced in this work by referencing [45–49]. Firstly, the performance of the designed radiometer is verified by measuring the temperature of water. Water is easy to obtain in nature, and its specific heat capacity is relatively large. Temperature variation of water is slow and uniform in the process of temperature decline, so the long-term performance and temperature sensitivity of the designed radiometer can be verified simultaneously. Then in order to test the response of the designed radiometer under clinical conditions, the temperature of swine skin tissue is measured.

To model the indoor environment, the designed radiometer is not placed in a microwave anechoic room, but directly in an ordinary room only with an air conditioning system. During the measurement process, no objects are allowed to move inside, and the air conditioning system is always working to keep the room temperature relatively constant.

3.1. Temperature Measurement of Water and Parameter Evaluations for Designed Radiometer

3.1.1. Temperature Measurement of Water

According to ITU-R [50], the normal direction emissivity of semi-infinite pure water within the physical temperature range of 0°C $\sim$ 80°C in Ku band varies in the range of 0.38 $\sim$ 0.41, which is relatively close to that of human skin.

Figure 9 shows the experimental setup. Water is placed in a beaker, and the horn antenna aperture is above water surface by **D1** = 70 mm. The aperture center of the horn antenna is aligned with the subface center of water. Values of η_M are obtained by simulation, as shown in Table 4. In order to verify the performance of the designed radiometer in indoor scenes, the environment is not shielded by any microwave absorber. Physical temperatures of water and reference noise source are measured in contact by two RTDs (PT100, TS1, and TS2), whose temperature sensitivities can reach 0.01 K. In order to prevent heat convection of water vapor from affecting the physical temperature of the antenna, an extremely thin plastic film with high wave permeability is placed on the water surface. As the indoor temperature is relatively constant during the measurement process, T_{pa}, T_{pl} and T_r are assumed to be equal to T_s, that is, $T_{pa} = T_{pl} = T_r = T_s$.

Table 4. Simulation results of weighting coefficient η_M for water in a beaker.

Distance $D1$ (mm)	Distribution Parameters	
	η_M	1-η_M
50	0.90294	0.09706
70	0.84528	0.15472
90	0.81130	0.18870
110	0.77957	0.22043
130	0.73655	0.26345

The actual measurement results and temperature inversion results of the microwave radiometer are shown in Figs. 9(b) and (c). The measurement time is about 2 hours. Recorded data points for each curve are more than 2000 in Figs. 9(b) (c). According to Fig. 9(c), the temperature inversion results basically coincide with the physical temperatures of the measured water. The designed radiometer has the ability to track water temperature changes.

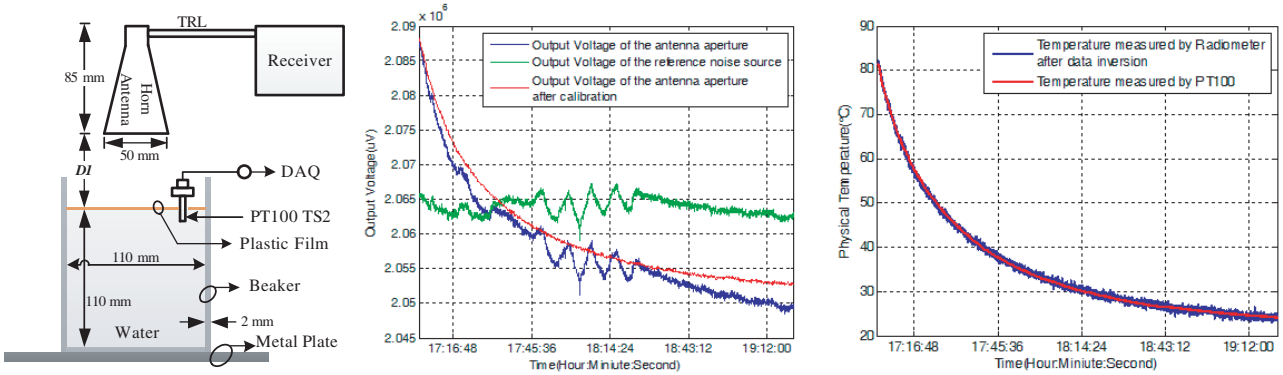

Figure 9. The measurement and calibration results of the water temperature by the designed radiometer with time. (a) Experimental setup; (b) Original measurement voltage data and calibrated voltage data; (c) Temperature inversion results of the microwave radiometer and physical temperatures measured by PT100 TS2.

3.1.2. Basic Parameter Evaluations of Designed Radiometer

Here, the temperature sensitivity and linearity of the designed radiometer are calculated. The corresponding relationship between output voltages calibrated by the reference noise source and the microwave apparent temperature of the measured water is plotted in Fig. 10(a). The linear regression analysis is carried out to calculate the linearity.

According to above test, the calculation method of the radiometer receiver sensitivity is as follows. Step 1: Gather all measured output voltages in all noise temperature input points, and calculate the average U and standard deviation σ of output voltages at each noise temperature input point. Step 2: Select two temperature point data randomly, and calculate the temperature sensitivity $\Delta T_{\min}$ of the receiver. The calculation formula is

$$\Delta T_{\min} = \frac{(\sigma_i + \sigma_j)}{2} \times \frac{T_i - T_j}{U_i - U_j} \tag{31}$$

Here, T_i and T_j are two temperature point data selected randomly, where $T_i \neq T_j$; U_i and U_j are measured output voltages; σ_i and σ_j are standard deviations for T_i and T_j, respectively.

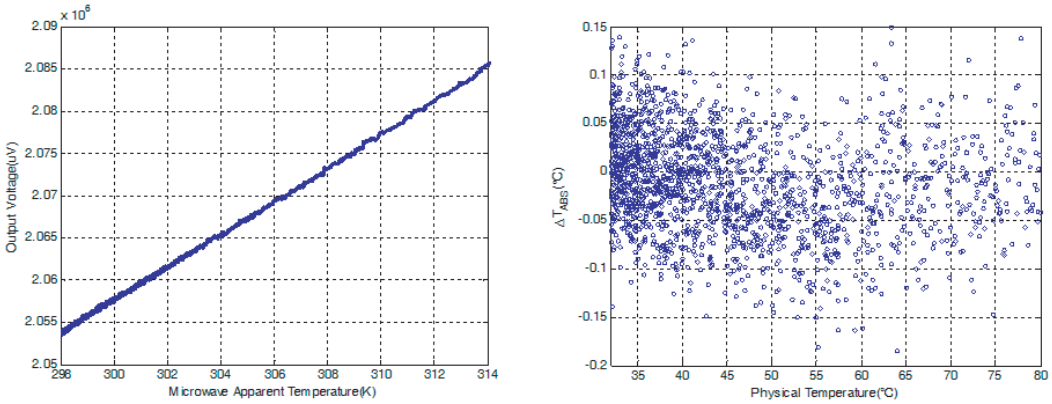

(a) (b)

Figure 10. (a) Corresponding relationship between output voltages calibrated by the internal calibration source and the microwave apparent temperature of the measured water. (b) Temperature measurement accuracy for pure water.

Then the absolute accuracy ΔT_{ABS} for the temperature of pure water measured by the radiometer can be expressed as

$$\Delta T_{ABS} = \bar{T} - T \tag{32}$$

Here, $\bar{T}$ is the physical temperature estimate after inversion by Equations (23)–(27), and T is the physical temperature measured by RTD PT100 TS2. According to Equation (32), the absolute accuracy for the temperature of pure water measured by the radiometer is plotted in Fig. 10(b). The basic parameters of the designed microwave radiometer are listed in Table 7.

3.2. Attenuation Caused by Cotton Cloth and Temperature Measurement through Cotton Cloth

Experiments are designed to verify the amplitude attenuation of Ku band microwave thermal radiation and infrared thermal radiation caused by cotton cloth and the temperature measurement performance of the designed microwave radiometer for the target sheltered by cotton cloth. The reason for choosing cotton cloth is that hospital gowns and quilts prepared for patients in EDs, ICUs, or general wards of hospitals are almost all made of cotton cloth and cotton fiber. The single layer thickness of the cotton cloth selected for the test is about 0.7 mm.

Experiments are carried out in three aspects: 1) Amplitude attenuation of infrared thermal radiation caused by cotton cloth. 2) Amplitude attenuation of Ku band microwave thermal radiation caused by cotton cloth. 3) The physical temperature measurement and inversion of water through cotton cloth by the designed microwave radiometer.

3.2.1. Amplitude Attenuation of Infrared Thermal Radiation Caused by Cotton Cloth

A calibrated infrared thermometer is used to measure apparent temperatures of water through cotton cloth. Water is placed in a high transmittance beaker. The infrared probe measures water from the right side of the beaker in order to reduce the influence of heat convection by water vapor on cotton cloth, so that the heat transfer mode is mainly heat radiation. Experimental setup is shown in Fig. 11(a).

The infrared probe is perpendicular to water surface through the wall of the beaker, and their positions are fixed. Measurement procedures are as follows. Step 1: Measure the apparent temperature of unsheltered water by the infrared thermometer. Step 2: Shelter water by cotton cloth rapidly and measure the apparent temperature of water through cotton cloth when cotton cloth stays for 2 s. Then cotton cloth is removed immediately. Step 3: Repeat Step 1 and Step 2 every 3 minutes for 12 times in total.

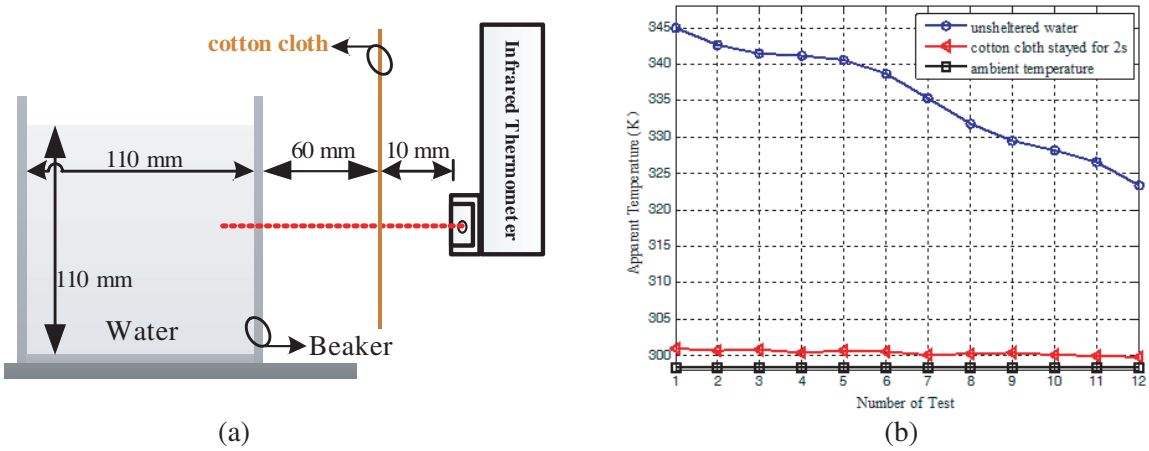

Figure 11. (a) Experimental setup; (b) Apparent temperature measurement results by the calibrated infrared thermometer. Here, the ambient temperature is about 25.2°C.

Measurement results are shown in Fig. 11(b). Phenomena can be observed as follows. (a) When water is unsheltered, the apparent temperature received by the infrared thermometer is decreased from about 345 K to 323 K over time. (b) When cotton cloth stays for 2 s between water and the infrared probe, the apparent temperature received by the infrared thermometer has only slight difference from room temperature and cannot follow apparent temperature changes of unsheltered water.

According to phenomena (a) and (b), the attenuation of infrared thermal radiation caused by cotton cloth is serious, which is above 0.90 [1, 2].

3.2.2. Amplitude Attenuation of Microwave Thermal Radiation Caused by Cotton Cloth

Because of microwave security applications, studies on the amplitude attenuation of microwave thermal radiation caused by common clothing materials are mostly concentrated in Ka band and above [1, 2], but studies are relatively few in Ku band.

In order to prove amplitude attenuation of Ku band microwave caused by cotton cloth, the designed radiometer is used to measure water through cotton cloth. The experimental setup is shown in Fig. 12(a).

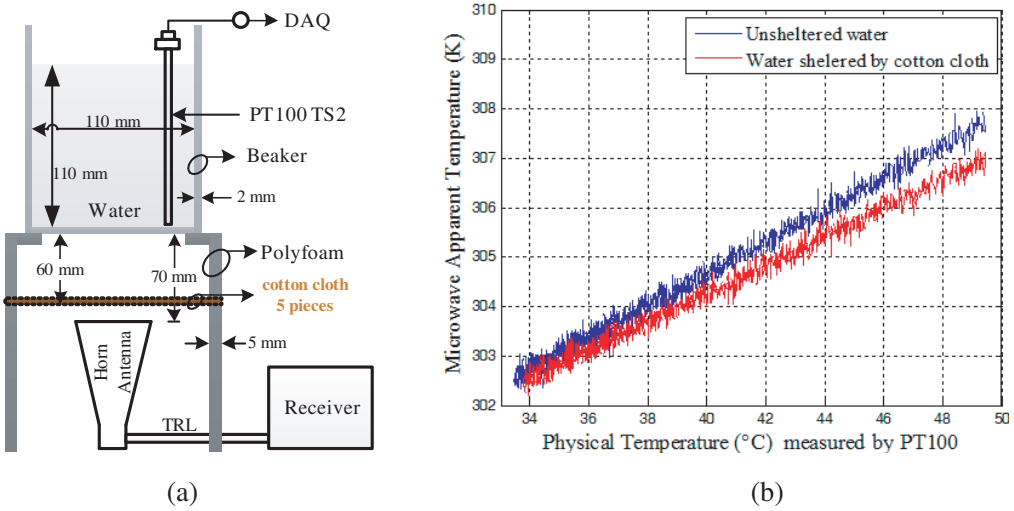

Figure 12. (a) Experimental setup; (b) Microwave apparent temperature measurement results for unsheltered water and water sheltered by 5 layers of cotton cloth.

To reduce the influence of heat convection on cotton cloth, the water is measured from the bottom of the beaker. The beaker has a high transmittance, which has negligible effect on the apparent temperature of water in Ku band. The antenna aperture is perpendicular to the water surface, and their positions are fixed.

Measurement procedures are as follows. Firstly, water sheltered by 5 layers of cotton cloth is measured. After that, cotton cloth is removed from Fig. 12(a) to measure the unsheltered water only. During two measurements, water is heated to 50°C and cooled naturally to 30°C over time. Physical temperatures of water are measured by RTD TS2.

Apparent temperatures measured by the designed radiometer are shown in Fig. 12(b). Both apparent temperatures of sheltered water and unsheltered water measured by the designed radiometer can follow physical temperature changes of water. By comparison, the slope of apparent temperature of the sheltered water is slightly lower than that of the unsheltered water, indicating that microwave thermal radiation emitted by water is attenuated by cotton cloth, but attenuation is small. After calculation, the attenuation of Ku band microwave caused by 5 layers of cotton cloth is about 0.02 (about 0.09 dB).

According to above measurements, attenuation caused by single-layer cotton cloth to infrared band is more than 10 dB, while that to Ku band microwave is about 0.02 dB. Compared to infrared band, cotton cloth is almost transparent to Ku band microwave.

3.2.3. Temperature Measurement of Water through Cotton Cloth by the Radiometer

According to above conclusions, water sheltered by 5 layers of cotton cloth is measured by the designed radiometer, and the temperature inversion is carried out by using the microwave thermal radiation transmission model of clothed human body.

The experimental setup is shown in Fig. 12(a) and Fig. 13(a). Temperature inversion results of the microwave radiometer and physical temperatures measured by PT100 TS2 are shown in Fig. 13(b). According to Fig. 13(b), temperature inversion results basically coincide with physical temperatures of water.

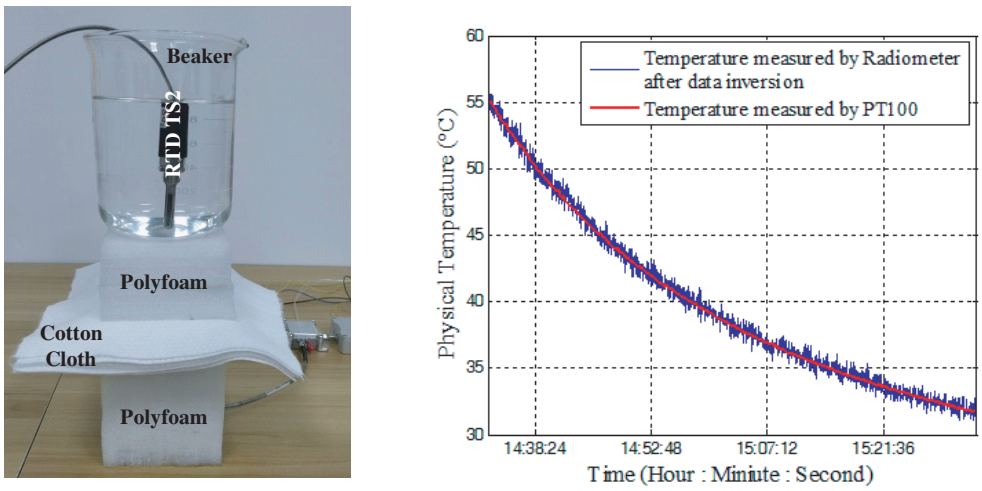

(a) (b)

Figure 13. (a) Photograph of the Experimental setup; (b) Temperature inversion results of the microwave radiometer and physical temperatures measured by PT100 TS2.

After calculation, when the temperature of water changes from 55.1°C to 31.5°C through cotton cloth, the noncontact temperature measurement accuracy is about ±0.3°C which is lower than that in Table 5. The reasons are as follows. The calculation model for the temperature of cotton cloth is different from its actual temperature. And there exists slight attenuation caused by cotton cloth for Ku band microwave.

Table 5. Swine skin tissue in test and Comparison with that of humans.

Biological tissue layer	Thicknesses of Biological Materials (mm)	
	Human skin tissue	Swine skin tissue in test
Skin	$0.8 \sim 4.5$	2.5
Hypodermis	$3.0 \sim 10.0$	8.0
Muscle and Fat	——	2.0

3.3. Temperature Measurements of Swine Skin Tissue through Cotton Cloth

In order to test the response of the designed radiometer to clothed human skin under clinical conditions, swine skin tissue covered with 2 layers of cotton cloth is measured, and the temperature measurement for uncovered swine skin tissue is used as a comparison group. In aspects of anatomical and physiological characteristics, swine skin is very similar to human skin, and the skin of swine aged 2 and 3 months is most similar to human skin [51–53]. Swine skin tissue can be heated and cooled rapidly by heating and refrigerating, which is conducive to observe change of skin temperature by the microwave radiometer in a short time. In reality, thicknesses of most cotton shirts are in the range of the 1.4 mm thickness of 2-layer cotton cloth.

As shown in Fig. 14(b), the biological tissue used in this experiment is swine chest skin tissue, which is composed of skin, hypodermis, some muscle, and fat, with a size about 20 cm $\times$ 20 cm $\times$ 1.25 cm, and thicknesses of all parts are shown in Table 5.

The block diagram and photographs of experimental setups are shown in Figs. 14(a), (b), (d), and $\mathbf{D} = 70$ mm. Measurement procedures were as follows. Step 1: Heat the swine skin tissue evenly in order that the overall temperature is close to 50°C. Step 2: Carry out temperature measurement for uncovered swine skin tissue in non-contact as shown in Fig. 14(b). Step 3: Repeat Step 1. Cover swine skin tissue with two-layer cotton cloth and carry out non-contact temperature measurement as shown in Fig. 14(d).

During the two measurements, an RTD PT100 is used to measure the skin-side physical temperature of swine skin tissue. The values of η_M are obtained by simulation, as shown in Table 6. Since swine skin tissue used in test is similar to human skin tissue, relevant parameters such as emissivity are assumed to be the same as human skin.

Table 6. Simulation results of weighting coefficient η_M for swine skin tissue.

Distance D (mm)	Distribution Parameters	
	η_M	1-η_M
50	0.98728	0.01272
70	0.96051	0.03949
90	0.91957	0.08043

Equations (28)–(30) are used for temperature inversion of test results in Figs. 14(b) and (d), respectively. Temperature inversion results are shown in Figs. 14(c) and (e). According to Fig. 14(e), after temperature inversion, non-contact temperature measurement results of covered swine skin tissue are basically consistent with its physical temperatures measured by RTD PT100. Compared with the results in Fig. 14(c), the accuracy of temperature measurement results in Fig. 14(e) is slightly worse which is about ± 0.3°C.

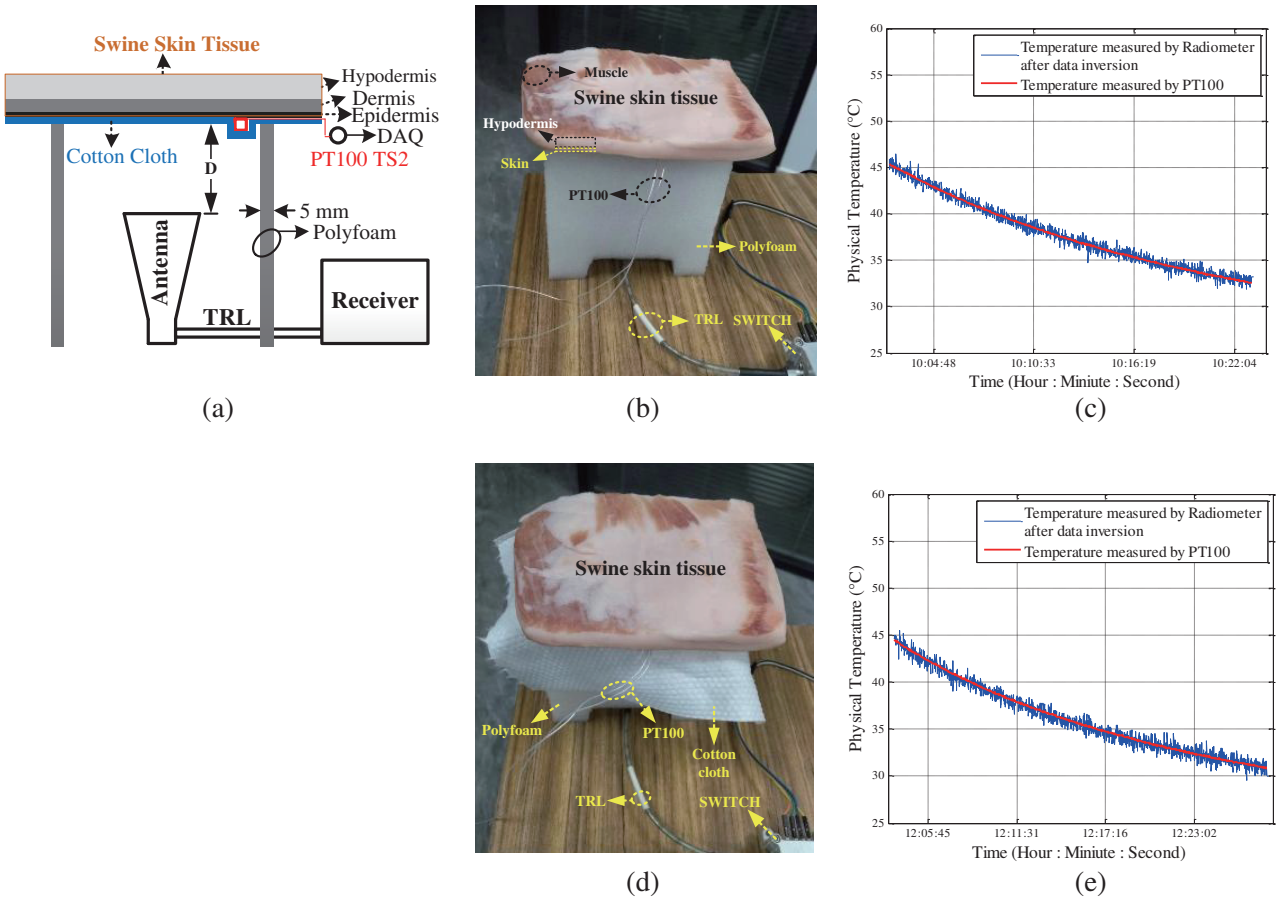

Figure 14. (a) Block diagram of the experimental setup; (b) Photograph of the experimental setup for uncovered swine skin tissue; (c) Measurement results for (b); (d) Photograph of the experimental setup for swine skin tissue covered by 2-layer cotton cloth; (e) Measurement results for (d).

Table 7. Basic parameters of the designed microwave radiometer.

Symbol	Basic Parameters
Working band	Ku
Integration time τ	≈ 1 s
Temperature sensitivity	≈ 0.08 K
Linearity	0.9996
Temperature accuracy	1) Pure Water: $\approx \pm 0.20$°C (59.8°C to 30.3°C);
	2) Water sheltered by 5-layer cotton cloth: $\approx \pm 0.30$°C (55.1°C to 31.5°C);
	3) Swine skin tissue: $\approx \pm 0.18$°C (45.1°C to 32.5°C);
	4) wine skin tissue covered by 2-layer cotton cloth: $\approx \pm 0.30$°C (44.5°C to 31.2°C).

4. DISCUSSION

This work is mainly focused on solving the problem of temperature measurement for critically ill patients in hospital EDs and ICUs. According to the practical requirement, a Ku band microwave radiometer is designed which can be conveniently used in measuring temperatures of patients' foreheads directly.

Notably, it can be applied to temperature measurements for patients' axillae or torsos through common clothes or quilts.

The designed microwave radiometer is a digital auto gain compensative microwave radiometer. Compared with the Dicke radiometer, the digital auto gain compensative microwave radiometer possesses a simpler receiver structure and a higher theoretical temperature measurement sensitivity. In this work, discrete circuit modules are used to verify the microwave radiometer design principle. Moreover, the miniaturized design and the assembled design are made for this radiometer. The temperature measurement sensitivity of the designed radiometer under non-ideal conditions is analyzed, and a novel compensation method related to the physical temperature of the internal reference noise source for receiver calibration is proposed to improve the temperature measurement sensitivity of the designed radiometer and reduce the frequency of external calibration in practice use. Furthermore, the microwave thermal radiation transmission model of clothed human body is proposed for physical temperature inversion of clothed human skin.

To demonstrate the performance of the designed radiometer for medical application standards, several experiments are conducted. For our purpose, firstly, unsheltered water is selected as the tested target, and the designed radiometer has the ability to track its physical temperature changes accurately after calibration and temperature inversion. Secondly, experiments are designed to verify the amplitude attenuation caused by cotton cloth of Ku band microwave and infrared thermal radiation, and the non-contact temperature measurement performance of the designed microwave radiometer for water sheltered by 5 layers of cotton cloth. The conclusion that amplitude attenuation caused by cotton cloth for Ku band microwave is much smaller than that for infrared thermal radiation is proven in this work by above experiment. Measurements show that temperature inversion results basically coincide with physical temperatures of sheltered water. Thirdly, medical temperature measurements are considered. A biological tissue, which is swine skin tissue, is selected for further testing. Results show that when it is uncovered or covered by cotton cloth, the designed radiometer can track both temperatures of swine skin tissue in above two conditions relatively accurately. Therefore, this designed radiometer does have advantages in measuring human skin temperature through clothing or quilts compared with infrared thermometers.

In aspects of working principle, system miniaturization design, temperature sensitivity derivation correction, temperature inversion model construction, and experimental confirmation, the microwave radiometer designed in our work is significantly different from those in [3–8, 45–49]. Researches mainly reported temperature measurements of human body internal tissues, and working frequency bands of microwave radiometers used were low [3–8, 24–28], so that antennas used must be carefully designed to reduce their sizes. In particular, temperature measurements are usually carried out using an antenna pressed against human skin in contact. In our work, the microwave radiometer designed is used to measure human skin temperature. The selected Ku band is much higher than those in [3–8, 45–49].

Table 8. Microwave radiometers above 9 GHz used for medical applications in references.

References	Basic Parameters				
	Working band	Bandwidth	Temperature sensitivity	Temperature accuracy	Measuring method
[14]	X band, CF*: 9.2 GHz	100 MHz	0.1 K	——	noncontact
[15–17]	X band, CF: 9.0 GHz	800 MHz	——	0.2°C	contact
[19]	X band, 9.0 ∼ 10.0 GHz	500 MHz	Order of 0.1 K	——	noncontact
[21]	Ka band, 32 ∼ 35 GHz	4 GHz	Order of 0.1 K	——	contact
[22]	X band, 10 ∼ 12 GHz	2 GHz	Order of 0.1 K	——	noncontact
[23]	Ku band, CF: 12.5 GHz	470 MHz	1.25 K	±4°C for an absorber load	noncontact
[24]	X band, 10.68 ∼ 10.70 GHz	20 MHz	≈ 0.5 K	——	noncontact

* CF means Centre Frequency.

The antenna used is a high directional horn antenna, and the measurement method is non-contact. On the other hand, although only a few researches were performed above 9 GHz for medical applications with microwave radiometers pertinent literatures [14–24] from the 1970s are also listed in Table 8 for comparisons of the designed radiometer in this work. These microwave radiometers reported in [14–24] are mainly used for body surface temperature measurement and imaging, breast cancer detection, detections of deep lesions such as those of femoral head or lumbar spine, or cerebral tumors, medical studies on occlusive vascular disease of the lower limbs, etc. On the basis of above researches, medical applications of microwave radiometers above 9 GHz are extended by our work. Meanwhile, the temperature sensitivity of the microwave radiometer for medical applications is further improved by our work.

In addition, further work is required to optimize the calibration algorithm, and more deviations are considered for the designed microwave radiometer. Importantly, clinical trials will also be conducted. In summary, this designed microwave radiometer shows great significance in medical applications for critical patients.

AUTHOR CONTRIBUTIONS

Conceptualization, H.T, Q.D. and J.M.; methodology, H.T. and J.M.; formal analysis, H.T.; investigation, H.T, X.Z. and A.H.; data curation, H.T.; writing-original draft preparation, H.T.; writing-review and editing, H.T. and J.M. All authors have read and agreed to the published version of the manuscript.

ACKNOWLEDGMENT

This research was funded by the National Natural Science Foundation of China (No. 6217012631).

REFERENCES

1. Bjarnason, J. E., T. L. J. Chan, A. W. M. Lee, et al., "Millimeter-wave, terahertz, and mid-infrared transmission through common clothing," *Applied Physics Letters*, Vol. 85, No. 4, 519–521, 2004.
2. Lin, S., *Microwave and Millimeter-Wave Remote Sensing for Security Applications*, 372 pages, Jeffrey A. Nanzer, Artech House, 2012, ISBN 978-1-60807-172-2[J].
3. Enander, B. and G. Larson, "Microwave radiometric measurements of the temperature inside a body," *Electronics Letters*, Vol. 10, No. 15, 317–317, 1974.
4. Barrett, A. H. and P. C. Myers, "Subcutaneous temperatures: a method of noninvasive sensing," *Science*, Vol. 190, No. 4215, 669–671, 1975.
5. Maruyma, K., S. Mizushina, T. Sugiura, et al., "Feasibility of noninvasive measurement of deep brain temperature in newborn infants by multifrequency microwave radiometry," *IEEE Transactions on Microwave Theory and Techniques*, Vol. 48, No. 11, 2141–2147, 2000.
6. Hand, J. W., G. M. J. Van Leeuwen, S. Mizushina, et al., "Monitoring of deep brain temperature in infants using multi-frequency microwave radiometry and thermal modelling," *Physics in Medicine & Biology*, Vol. 46, No. 7, 1885, 2001.
7. Popovic, Z., R. Scheeler, P. Momenroodaki, et al., "Microwave thermometer for internal body temperature retrieval," U.S. Patent Application 15/608,284[P], Nov. 30, 2017.
8. Momenroodaki, P., W. Haines, M. Fromandi, et al., "Noninvasive internal body temperature tracking with near-field microwave radiometry," *IEEE Transactions on Microwave Theory and Techniques*, Vol. 66, No. 5, 2535–2545, 2018.
9. McGrath, J. A., R. A. J. Eady, and F. M. Pope, "Anatomy and organization of human skin," Rook's textbook of dermatology, Vol. 1, 3.2–3.80, 2004.
10. Black, D., J. Vora, M. Hayward, et al., "Measurement of subcutaneous fat thickness with high frequency pulsed ultrasound: Comparisons with a caliper and a radiographic technique," *Clinical Physics and Physiological Measurement*, Vol. 9, No. 1, 57, 1988.

11. Gabriel, C., S. Gabriel, and E. Corthout, "The dielectric properties of biological tissues: I. Literature survey," *Physics in Medicine & Biology*, Vol. 41, No. 11, 2231–2249, 1996.
12. Gabriel, S., R. W. Lau, and C. Gabriel, "The dielectric properties of biological tissue II: Measurements in the frequency range 10 Hz to 20 GHz," *Physics in Medicine and Biology*, Vol. 41, No. 11, 2251–2269, 1996.
13. Gabriel, S., R. W. Lau, and C. Gabriel, "The dielectric properties of biological tissues: III. Parametric models for the dielectric spectrum of tissues," *Physics in Medicine & Biology*, 41, 1996.
14. Bigu-Del-Blanco, J., C. Romero-Sierra, and J. A. Tanner, "Some theory and preliminary experiments on microwave radiometry of biological systems," *S-MTT International Microwave Symposium Digest*, 41–44, 1974.
15. Mamouni, A., Y. Leroy, M. Samsel, and M. Gautherie, "Radiothermométrie micro-onde à 9 GHz: Applications aux cancers du sein et à des localisations tumorales diverses. Résultats préliminaires," *Microwave Power Symposium 1979, XIVe Symposium International sur les Applications énergétiques des Micro-ondes*, Monaco, Jun. 11–15, 1979.
16. Mamouni, A., D. D. N'Guven, M. Robillard, M. Chive, and Y. Leroy, "Physical basis and technology of microwave radiometry," *Proc. SPIE 0211, Optics and Photonics Applied to Medicine*, May 29, 1980, https://doi.org/10.1117/12.958370.
17. Gautherie, M., A. Mamouni, M. Samsel, J. L. Guerquin-Kern, Y. Leroy, and C. Gros, "Microwave radiothermometry (9 GHz) applied to breast cancer," *Proc. SPIE 0211, Optics and Photonics Applied to Medicine*, May 29, 1980, https://doi.org/10.1117/12.958372.
18. Robert, J., J. Edrich, Y. Leroy, A. Mamouni, J. M. Escanye, and P. Thouvenot, "Clinical applications of microwave thermography," *Proc. SPIE 0211, Optics and Photonics Applied to Medicine*, May 29, 1980, https://doi.org/10.1117/12.958371.
19. Abdul-Razzak, M. M., B. A. Hardwick, G. L. Hey-Shipton, et al., "Microwave thermography for medical applications," *IEE Proceedings A (Physical Science, Measurement and Instrumentation, Management and Education, Reviews)*, Vol. 134, No. 2, 171–174, 1987.
20. Poikalainen, V. and J. Praks, "The use of microwave thermometer for the determination of cows' body surface temperature," *Transactions of the Estonian Academic Agricultural Society (Estonia)*, 1998.
21. Kanakov, V. A. and A. G. Kislyakov, "Human-body temperature measurements using contact radiometer with built-in calibrators," *Radiophysics & Quantum Electronics*, Vol. 42, No. 2, 150–156, 1999.
22. Tipa, R. and O. Baltag, "Microwave thermography for cancer detection," *Romanian Journal of Physics*, Vol. 51, Nos. 3/4, 371, 2006.
23. Stephan, K. D., J. B. Mead, D. M. Pozar, et al., "A near field focused microstrip array for a radiometric temperature sensor," *IEEE Transactions on Antennas and Propagation*, Vol. 55, No. 4, 1199–1203, 2007.
24. David, J. I., M. B. Zemel, C. T. Lyster, and N. Feld, "Passive microwave assessment of human body core to surface temperature gradients and basal metabolic rate," USA, US 8,013,745 B2[P], Sep. 6, 2011.
25. Zhao, K., J. X. Shi, and H. D. Zhang, "High sensitivity airborne l-band microwave radiometer measurements of sea surface salinity," *Journal of Remote Sensing*, 2008, DOI: 10.3321/j.issn:1007-4619.2008.02.012.
26. Jian, S., Z. Kai, J. Tao, et al., "A new airborne Ka-band double-antenna microwave radiometer for cloud liquid water content measurement," *Proceedings of SPIE — The International Society for Optical Engineering*, Vol. 8866, 17, 2013.
27. Ulaby, F. T., R. K. Moore, and A. K. Fung, "Microwave remote sensing: Active and passive. Volume 1 — Microwave remote sensing fundamentals and radiometry," *Remote Sensing A*, Vol. 2, No. 5, 355–356, 1981.
28. Wohlleben, R., H. Mattes, and O. Lochner, "Simple small primary feed for large opening angles and high aperture efficiency," *Electronics Letters*, Vol. 8, No. 19, 474–476, Sep. 21, 1972.

29. Milligan, T. A., *Modern Antenna Design*, 2nd Edition, Wiley, 2005.
30. James, G. L., "Radiation properties of 90° conical horns," *Electronics Letters*, Vol. 13, No. 10, 293–294, May 12, 1977.
31. Silver, S., *Microwave Antenna Theory and Design*, Chapter 11, 1984.
32. Clarricoats, P. J. B. and P. K. Saha, "Radiation pattern of a lens-corrected conical scalar horn," *Electronics Letters*, Vol. 5, No. 23, 592–593, Nov. 1969.
33. Neto, A., S. Maci, P. J. I. de Maagt, "Reflections inside an elliptical dielectric lens antenna," *IEE Proceedings — Microwaves, Antennas and Propagation*, Vol. 145, No. 3, 243-247, Jun. 1998.
34. Pohl, N., "A dielectric lens antenna with enhanced aperture efficiency for industrial radar applications," *EEE Middle East Conference on Antennas and Propagation (MECAP 2010)*, 1–5, 2010.
35. van der Vorst, M. J. M., P. J. L. de Maagt, and M. H. A. J. Herben, "Effect of internal reflections on the radiation properties and input admittance of integrated lens antennas," *IEEE Transactions on Microwave Theory and Techniques*, Vol. 47, No. 9, 1696–1704, Sep. 1999.
36. Nguyen, N. T., R. Sauleau, and C. J. M. Perez, "Very Broadband Extended Hemispherical Lenses: Role of Matching Layers for Bandwidth Enlargement," *IEEE Transactions on Antennas and Propagation*, Vol. 57, No. 7, 1907–1913, Jul. 2009.
37. https://www.pasternack.cn/wr-62-waveguide-gain-horn-antenna-15db-square-flange-pewan062-15-p.aspx.
38. https://www.pasternack.cn/wr-62-waveguide-standard-gain-horn-antenna-15-dbi-sma-pewan062-15elsf-p.aspx.
39. Pozar, D. M., *Microwave Engineering*, 4th Edition, Wiley, New York, NY, USA, 2012.
40. Holmes, J., C. Balanis, and W. Truman, "Application of Fourier transforms for microwave radiometric inversions," *IEEE Transactions on Antennas and Propagation*, Vol. 23, No. 6, 797–806, 1975.
41. Truman, W., C. Balanis, and J. Holmes, "Three-dimensional vector modeling and restoration of flat finite wave tank radiometric measurements," *IEEE Transactions on Antennas and Propagation*, Vol. 25, No. 1, 95–104, 1977.
42. Li, Q., G. Wei, Z. Zhang, et al., "Brightness temperature of extended targets," *ICMMT'98. 1998 International Conference on Microwave and Millimeter Wave Technology Proceedings (Cat. No.98EX106)*, 483–487, 1998.
43. Li, Q., G. Wei, Z. Zhang, et al., "Models for the brightness temperature of extended targets at MM wave frequency,". *International Journal of Infrared and Millimeter Waves*, Vol. 19, No. 9, 1247–1253, 1998.
44. Xiao, Z., J. Xu, and T. Hu, "Research on the transmissivity of some clothing materials at millimeter-wave band," *2008 International Conference on Microwave and Millimeter Wave Technology*, 1750–1753, 2008.
45. Susek, W., "Thermal microwave radiation for subsurface absolute temperature measurement," *ACTA Phys. Pol. A*, Vol. 118, 1246–1249, 2010.
46. Momenroodaki, P., Z. Popovic, and R. Scheeler, "A 1.4-GHz radiometer for internal body temperature measurements," *2015 European Microwave Conference (EuMC)*, 694–697, Paris, France, Sep. 7–10, 2015.
47. Jacobsen, S. and O. Klemetsen, "Improved detectability in medical microwave radio-thermometers as obtained by active antennas," *IEEE Trans. Biomed. Eng.*, Vol. 55, 2778–2785, 2008.
48. Bonds, Q., J. Gerig, T. M. Weller, and P. Herzig, "Towards core body temperature measurement via close proximity radiometric sensing," *IEEE Sensors Journal*, Vol. 12, 519–526, 2012.
49. Klemetsen, O., Y. Birkelund, S. K. Jacobsen, P. F. Maccarini, and P. R. Stauffer, "Design of medical radiometer front-end for improved performance," *Progress In Electromagnetics Research B*, Vol. 27, 289–306, 2011.
50. International Telecommunication Union Radiocommunication Assembly, "Attenuation Due to Clouds and Fog," Recommendation ITU-R P.840-8, 2019.

51. Mcintyre, M. K., B. Baker, T. J. Peacock, et al., "Initial characterization of the pig skin bacteriome and its effect on in vitro models of wound healing," *The FASEB Journal*, 30, 2016.
52. Abd, E., S. A. Yousef, M. N. Pastore, et al., "Skin models for the testing of transdermal drugs," *Research & Reports in Transdermal Drug Delivery*, Vol. 8, 163–176, 2016.
53. Paul, H., A. Jon, M. Krysta, et al., "Vital, porcine, gal-knockout skin transplants provide efficacious temporary closure of full-thickness wounds: Good laboratory practice-compliant studies in nonhuman primates," *Journal of Burn Care & Research*, Vol. 41, No. 2, 229–240, Official Publication of the American Burn Association, 2020.